PCCP

Cite this: *Phys. Chem. Chem. Phys.*, 2011, **13**, 8869–8880

www.rsc.org/pccp

PAPER

Unraveling the flavin-catalyzed photooxidation of benzylic alcohol with transient absorption spectroscopy from sub-pico- to microseconds

Uwe Megerle,[a] Matthias Wenninger,[a] Roger-Jan Kutta,[b] Robert Lechner,[c] Burkhard König,[c] Bernhard Dick[b] and Eberhard Riedle*[a]

Received 21st January 2011, Accepted 23rd February 2011
DOI: 10.1039/c1cp20190e

Flavin-mediated photooxidations have been described for applications in synthetic organic chemistry for some time and are claimed to be a route to the use of solar energy. We present a detailed investigation of the involved photophysical and photochemical steps in methoxybenzyl alcohol oxidation on a timescale ranging from sub-picoseconds to tens of microseconds. The results establish the flavin triplet state as the key intermediate for the photooxidation. The initial step is an electron transfer from the alcohol to the triplet state of the flavin catalyst with $^3k_{ET} \approx 2 \times 10^7$ M^{-1} s^{-1}, followed by a proton transfer in $\sim$6 μs. In contrast, the electron transfer involving the singlet state of flavin is a loss channel. It is followed by rapid charge recombination (τ = 50 ps) without significant product formation as seen when flavin is dissolved in pure benzylic alcohol. In dilute acetonitrile/water solutions of flavin and alcohol the electron transfer is mostly controlled by diffusion, though at high substrate concentrations >100 mM we also find a considerable contribution from preassociated flavin–alcohol-aggregates. The model including a productive triplet channel and a competing singlet loss channel is confirmed by the course of the photooxidation quantum yield as a function of substrate concentration: We find a maximum quantum yield of 3% at 25 mM of benzylic alcohol and significantly smaller values for both higher and lower alcohol concentrations. The observations indicate the importance to perform flavin photooxidations at optimized substrate concentrations to achieve high quantum efficiencies and provide directions for the design of flavin photocatalysts with improved performance.

1. Introduction

Riboflavin, vitamin B_2, is an important biological redox cofactor capable of two subsequent one electron transfers.[1] Due to its reasonably strong absorption up to 500 nm and the redox properties of its excited states it has been used as a chemical photocatalyst operating with visible light. Flavin-based photoredox systems were inspired by the biological model of photolyase, a light driven bacterial enzyme repairing thymine dimer DNA lesions by photoinduced single electron transfer. Its mode of action has been investigated and mimicked by several model systems. The studies revealed the photocatalytic one electron repair mechanism and the dependence of the efficiency on the distance of the reduced flavin and additional sensitizing chromophores.

Preparative flavin-mediated photooxidations[2,3] were investigated by Shinkai,[4,5] Fukuzumi[6–8] and others.[9–12] To enhance the photocatalytic efficiency and photocatalyst stability, heterocyclic substrate binding sites or flavin transition metal complexes have been used. The redox properties of flavin were modulated by hydrogen bonding and transition metal complexation.[13–16] Scandium complexes of flavin without a detailed described structure were used by Fukuzumi to investigate photophysical parameters and propose a mechanistic scheme of the process. Some of us have used zinc-cyclen appended flavins for the photooxidation of benzyl alcohols[17] and recently extended the synthetic scope to photocatalytic cleavage of benzyl protection groups and photooxidation of activated hydrocarbons by flavin tetraacetate and blue light.[18]

Flavin photocatalysts reported so far were designed on the assumption that close proximity of the substrate and flavin chromophore will enhance the efficiency and selectivity of the photooxidation process. This assumption is based on the well known distance dependence of electron transfer as described by the Marcus theory and successful examples from template photochemistry.[19] However, our preliminary quantum yield determinations of the flavin photooxidation at different substrate

[a] *Lehrstuhl für BioMolekulare Optik, Ludwig-Maximilians-Universität München, 80538 München, Germany. E-mail: riedle@physik.lmu.de; Fax: +49 89 2180 9202; Tel: +49 89 2180 9210*
[b] *Institut für Physikalische und Theoretische Chemie, Universität Regensburg, D-93040 Regensburg, Germany*
[c] *Institut für Organische Chemie, Universität Regensburg, D-93040 Regensburg, Germany*

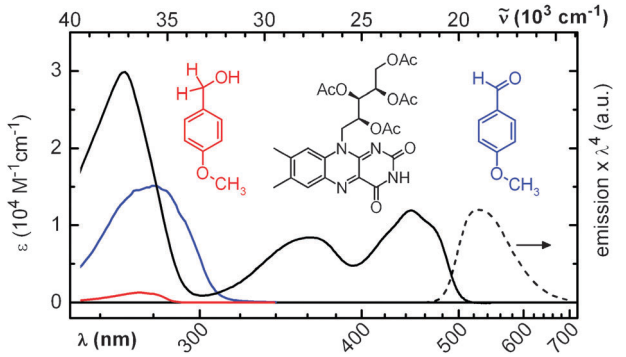

Fig. 1 Steady state absorption spectra of the oxidized form of riboflavin tetraacetate (RFTA, black), 4–methoxybenzyl alcohol (MBA, red) and 4-methoxy-benzaldehyde (blue) dissolved in MeCN/H_2O (50 : 50, v/v). The emission spectrum of RFTA is shown as a dashed line. The wavelength scale is reciprocal to render a linear energy scale shown at the top.

concentrations indicated that this assumption is not generally valid.[20] Therefore it seems necessary to reinvestigate the flavin mediated benzyl alcohol photooxidation with state-of-the-art time resolved spectroscopic methods.

The photophysical properties of flavins have been studied for almost a century.[21,22] In the past decade, transient absorption studies with picosecond to microsecond resolution have been carried out in solution[23–26] and in protein environment[27–33] to gain insight into the excited state dynamics of flavin-based systems. The experimental studies have been assisted by various *ab initio* calculations.[34–40] In many cases, the first step of the photo-initiated dynamics consists of an ultrafast electron transfer from a donor to the excited flavin.

In the present paper we aimed at gaining a complete understanding of the photooxidation mechanism of 4–methoxybenzyl alcohol (MBA) to the corresponding aldehyde using riboflavin tetraacetate (RFTA) as catalyst (Fig. 1). We found that relevant processes during the reaction occur both in the singlet and triplet manifold of RFTA states. Therefore, the timescales for the productive reactions and loss channels range from sub-picoseconds to several microseconds. To measure the fast singlet dynamics we used a setup based on a femtosecond white light pulse as a probe, while the slower triplet dynamics were monitored with a Streak camera using a pulsed Xe-flashlamp to generate the probe light. This unique combination of state-of-the-art spectrometers renders a detailed picture of the flavin photoreaction and thereby helps to derive structural design guidelines for photocatalysts with improved performance.

2. Experimental section

Riboflavin tetraacetate (RFTA) was synthesized as previously reported.[12] 4–methoxybenzyl alcohol (MBA) was obtained from Acros and distilled before use. The solvents acetonitrile (MeCN), water and DMSO were of spectroscopic quality. The steady state spectra were recorded with a Perkin-Elmer Lambda 19 spectrophotometer and a Spex Fluorolog 2 spectrofluorometer at room temperature. For the fluorescence measurements, the optical density of the sample in a 1 cm cuvette was 0.05 at the excitation wavelength of 420 nm. The fluorescence spectrum was corrected for the instrument response and multiplied by a factor of λ^4 to obtain the spectral shape of the stimulated emission in the time resolved absorption spectra.[41]

Femtosecond transient absorption measurements

The femtosecond spectrometer has been described in detail.[42] A Ti:sapphire amplifier system (CPA 2001; Clark MXR) was used to pump a noncollinear optical parametric amplifier tuned to 480 nm. The pulses were compressed to ~50 fs and attenuated to 400 nJ at the sample position. By focusing another part of the Ti:sapphire laser into a moving CaF_2 disk (4 mm thickness), a probe white light was generated ranging from below 300 nm to 750 nm. A computer controlled delay line was used to set pump–probe delays up to 1 ns. The pump and probe pulses were focused into the sample to spot sizes of 120 μm and 30 μm FWHM using spherical mirrors. After the interaction in the sample, the probe beam was dispersed with a fused silica prism and detected with a photodiode array of 512 pixels. The relative polarizations between the pump and probe were set to the magic angle (54.7°) by a half-wave plate in the pump-beam path. The ~1.5 ps chirp of the white light was corrected for prior to the data analysis using the coherent artifact as an indicator for time zero at each wavelength. Throughout the probe range, the spectral resolution was better than 100 cm^{-1} and the temporal resolution was better than 150 fs. For the experiments in MeCN/H_2O (50 : 50, v/v) solution, the temperature of the sample was set to 300 K. A flow cell with 1 mm thickness was used and the flavin concentration was 0.5 mM. The measurements in pure MBA and in MeCN/DMSO (98 : 2, v/v) were performed with a flow cell of 120 μm thickness at ambient temperature. Here, the flavin concentration was 2 mM.

Microsecond transient absorption measurements

To measure transient spectra in the range from nanoseconds to 20 μs the sample was excited with 8–10 ns pulses at 450 nm from a 10 Hz Optical Parametric Oscillator (OPO, Continuum) pumped by the third harmonic of a Nd:YAG laser (Surelite II, Continuum). A pulsed 150 W Xe flashlamp (MSP-05, Müller Elektronik-Optik) was used as probe light and the full time range was monitored at once with a streak camera (C7700, Hamamatsu Photonics).[32] RFTA was dissolved in MeCN/H_2O (50 : 50, v/v) at a concentration of 40.9 μM, which gave an optical density of about 0.5 at 450 nm with a path length of 10 mm. A fused silica flow cuvette with 10 mm of optical path length for excitation and 10 mm for probe light was used. Including the storage vessel and the peristaltic pump, the overall volume was 10 mL. The excitation light was focused into the sample with a cylindrical lens (f = 150 mm), and the pulse energy was adjusted to about 8 mJ per pulse at the sample. Mechanical shutters were used to select pump and probe pulses. The probe light with a very flat intensity profile of 2 ms duration was refocused three times by a series of toric mirrors: on a mechanical shutter to block the continuous light from the Xe flashlamp, on the sample cell, and on the entrance slit of the imaging spectrograph (Bruker 200is, grating 100 grooves per mm) in front of the streak camera.

The streak camera converts the coupled spectral and temporal information into two-dimensional images of the intensity distribution of the probe white light. Each transient absorption data set was calculated from four images taken with a frequency of 0.5 Hz: an image (D_{FL}) with both flash lamp and laser, an image (D_0) without any incoming light, an image (D_F) only with the flash lamp, and an image (D_L) only with the laser. Results represent the average of 100 individual measurement sequences with a time window of 10 μs and a time resolution of 20 ns. The transient absorption is calculated from these data as $\log[(D_F - D_0)/(D_{FL} - D_L)]$. The fluorescence of RFTA can be very strong, much brighter than the white light pulse. In this case the fluorescence is not cancelled well in the difference $D_{FL} - D_L$ and we used D_0 instead of D_L as the background for the data D_{FL}. The data analysis then yields the fluorescence spectrum as an additional component with unresolved decay time. All described measurements were performed at ambient temperature.

Data analysis

Data were analyzed with homemade software to obtain decay associated difference spectra (DADS). This analysis corresponds to the least-squares fit:

$$|\Delta\mathrm{OD}(t,\lambda) - \sum_{k}^{N} f_k(t)\mathrm{DADS}_k(\lambda)|^2 = \min, \qquad (1)$$

where $\Delta\mathrm{OD}(t, \lambda)$ is the measured data matrix and the $f_k(t)$ are exponential (or more complex) decay functions convoluted with a Gaussian function as the apparatus response function $g(t)$

$$f_k(t) = g(t) \otimes \exp(-(t - t_0)/\tau_k). \qquad (2)$$

For each manifold $\{f_k\}$ the DADS display the spectral changes associated with the particular decay times τ_k. This procedure does not assume a specific kinetic model assigning the rates to reaction steps, but is compatible with all models that involve only unimolecular reaction steps. The DADS are in turn linear combinations of the species spectra. The linear coefficients depend on the particular kinetic model, *e.g.*, a linear decay sequence or models involving parallel reactions and branching. After a kinetic model has been chosen, the system of linear equations can be solved for the species spectra.

Quantum yields

Relative product quantum yields (QY) for different MBA concentrations in MeCN/H_2O (50 : 50, v/v) were determined by the change in the absorbance in the region of 305 to 325 nm. In this region the absorbance of the product 4-methoxybenzaldehyde is much larger than that of MBA, and the contribution of RFTA is constant (compare Fig. 1). Photoexcitation was performed in fused silica cuvettes with a 2 mm by 10 mm cross section. Two high-power LEDs (Luxeon III Emitter LXHL-PBO9, Philips, 150 mW at 460 nm) were mounted at 1 cm distance to each other on opposite sides of the cuvette. The path length for monitoring the changing absorption was 10 mm, for photoexcitation 2 mm. A custom-designed power supply was used to apply light pulses of reproducible length and intensity. Absorption spectra were measured with a Perkin Elmer Lambda-9 spectrometer. The temperature of the cuvette was held at 20 °C by a thermostat.

Absolute values for the product QYs were obtained by calibration of the maximum value at 25 mM MBA using an LED-based apparatus described in detail elsewhere.[20] Here, the RFTA concentration was set to 2 mM as in the femtosecond experiments. After a defined irradiation time with 20.2 mW of 443 nm light, the chemical yield of 4-methoxybenzaldehyde was determined by quantitative gas chromatography. From the number of absorbed photons and the resulting chemical conversion, the absolute reaction quantum yield was determined.

3. Results and discussion

The spectroscopic study of the flavin-catalyzed photooxidation of benzylic alcohol relies on the differing spectra of the various redox and protonation states of flavin. All existing models assume that essentially only the catalyst and the substrate contribute to the reaction steps. Consequently we can deduce the oxidation mechanism from the time resolved observation of the evolving flavin transformation.

3.1 Femtosecond dynamics of riboflavin tetraacetate in pure methoxybenzyl alcohol

The simplest and seemingly clearest approach to study the photocatalytic oxidation is to bring the substrate MBA and the catalyst RFTA in direct contact. Typically, one would assume that this system shows the most effective conversion of alcohol to aldehyde since the reactants are inevitably in close proximity. However, we find that the experimental results contradict this assumption.

Even so MBA solidifies at room temperature, the lowering of the melting point by the solute is already sufficient to turn it into a highly viscous liquid that easily dissolves RFTA in mM concentrations. Thus, we could perform transient absorption measurements at ambient temperature in a flow cell without any additional solvent. Fig. 2a shows the transient absorption spectra of RFTA dissolved in pure MBA between −1 and 1000 ps after excitation at 480 nm, the first absorption maximum of flavin. The spectra consist of three major contributions that can all be assigned to RFTA transitions. Two bands with negative changes of the optical density indicate the ground state bleach (GSB) of RFTA around 450 nm and the stimulated emission (SE) around 560 nm. These bands are partially overlaid with the excited state absorption (ESA) that contributes a positive absorption change and has its maximum around 370 nm. All of these signatures decay to the baseline within the observed time window indicating a complete deactivation back to the ground state of RFTA on the timescale of several tens of picoseconds.

A closer inspection of the data reveals a significantly faster decay of the SE around 560 nm than of the ESA or GSB bands. This is clearly seen in Fig. 2b. The few ps decay of the stimulated emission goes along with an apparent redshift of the ESA band by ~10 nm. The GSB, however, shows no significant dynamics on this timescale. Except for minor shifts and the missing SE band, the transient spectrum after the fluorescence quenching (at a delay time Δt = 10 ps) is similar

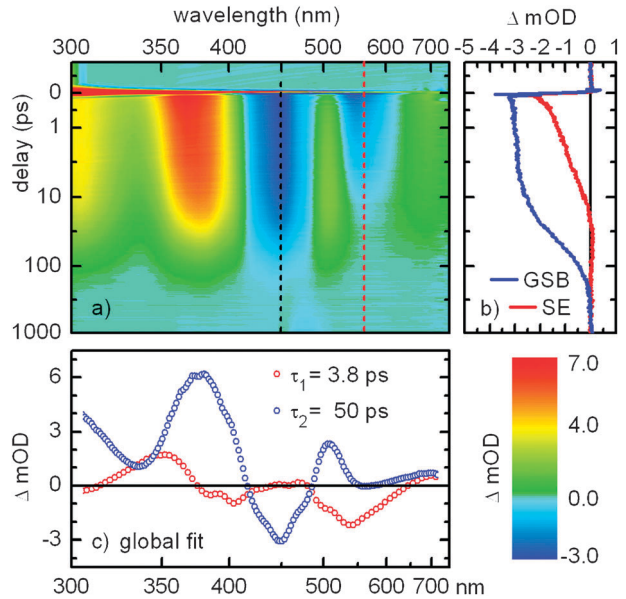

Fig. 2 (a) Transient absorption of RFTA dissolved in pure methoxybenzyl alcohol after excitation at 480 nm. The delay time axis is linear between −1 and 1 ps and logarithmic between 1 and 1000 ps. (b) Kinetic traces show a faster decay in the band of the stimulated emission (SE, 560 nm, red line) than in the ground state bleach (GSB, 450 nm, blue line). (c) Decay associated difference spectra from a biexponential global fit.

to the transient spectrum of the S_1 state (Δt = 0 ps). This situation is frequently found when the quenching mechanism is an electron transfer to the excited chromophore. Typically, the low energy transitions from the S_1 state involve the promotion of the electron from the highest SOMO (corresponding to the LUMO of the equilibrium molecule) to higher unoccupied orbitals. In first approximation, these transitions are not affected when an additional electron is transferred to the lower lying SOMO of the S_1 state (corresponding to the HOMO). Consistently, the observed spectral features agree well with the absorption spectrum of the flavin radical anion.[43]

This proves that the first step of the photoinduced dynamics is an electron transfer (ET) from one of the surrounding MBA molecules to ^{1}RFTA* yielding the radical anion RFTA$^{\bullet-}$ and the radical cation MBA$^{\bullet+}$. The weak signature of the radical cation expected around 440 nm[44–46] is not observed spectroscopically as it is masked by the much stronger ground state bleach of flavin. The absence of any residual signals at long delay times indicates a full charge recombination by back electron transfer from RFTA$^{\bullet-}$ to MBA$^{\bullet+}$.

In a precise description, the ET process described above changes the ESA band of ^{1}RFTA* into a very similar product absorption of RFTA$^{\bullet-}$. Due to the spectral similarity and the nearly identical intensity, we choose to use the term "ESA band" for the denomination of both.

To quantify the dynamics of the ET processes, we perform a least square global analysis using a biexponential fit function. We find that the spectral evolution can be well reproduced with two decay time constants of 3.8 and 50 ps. The decay associated difference spectra shown in Fig. 2c underline the qualitative description given above. The fast time constant is negligible in the region of the GSB, but forms the strongest contribution in the SE band. The dispersive shape of the amplitude spectrum around 370 nm again shows the fast spectral shift of the ESA band. In contrast, the decay associated difference spectrum of the 50 ps component has a very low amplitude in the SE band, but reflects the concerted decay of ESA and GSB.

Thus, after photoexcitation, the system of RFTA in pure MBA performs a nonproductive cycle of fast forward ET (~4 ps), but also rapid back-ET (50 ps) that restores the reactants RFTA and MBA to the ground state. It is noteworthy that the triplet state ^{3}RFTA does not play a role under these conditions as the known rate of intersystem crossing[39,47] is about three orders of magnitude smaller than the competing S_1 quenching rate of ~$(4\ \text{ps})^{-1}$. The fast back-reaction essentially rules out any further electron or proton transfer steps from MBA to RFTA needed to convert the alcohol to aldehyde. From the photocatalytic point of view, dissolving RFTA directly in the substrate MBA inhibits an effective utilization of photons, *i.e.* a good photoreaction quantum yield. The results from the ultrafast spectroscopic analysis explain why practically no conversion of MB-alcohol to MB-aldehyde can be observed even under long-time irradiation. To reach traceable aldehyde concentrations in an alcohol environment requires so many excitations per RFTA molecule that the flavin will likely degrade before.

3.2 Femtosecond dynamics in a dilute solution of MeCN/DMSO

As shown in the previous section, a direct contact between MBA and RFTA is not desirable for efficient photocatalysis. To circumvent this we used the "inert" solvent acetonitrile (MeCN) to dissolve RFTA and MBA in chosen concentrations. For better solubility of RFTA (up to 2 mM), we added 2 vol.% of DMSO to MeCN. By changing the MBA concentration one can then tune the average distance between the reactants. Based on the strong distance dependence of electron transfer one can also expect the rates to decrease significantly.

The transient absorption spectra of RFTA in solution are very similar to the ones in pure MBA. As shown in Fig. 3a, they consist of the same signatures, most prominently a strong ESA band around 360 nm, the negative GSB around 440 nm and the negative SE band around 550 nm. Small differences in the shape and position of these bands with respect to the ones observed in pure MBA can be explained by the lower polarity of the MeCN/DMSO mixture.[48]

In the absence of MBA, our time window of 1 ns allows for the observation of only the onset of a slow decay of all signals. This decay reflects the photophysical lifetime of the S_1 state of flavin. With time correlated single photon counting we can determine the fluorescence lifetime of RFTA with higher accuracy and find a value of 6.0 ns, very similar to other flavins in solution.[26] Upon addition of MBA in concentrations of several hundred mM, one observes an increasingly faster decay of all signatures. For example, at 300 ps delay and 400 mM MBA, the amplitude of the RFTA signals has dropped to 50% of the initial value directly after excitation (Fig. 3a).

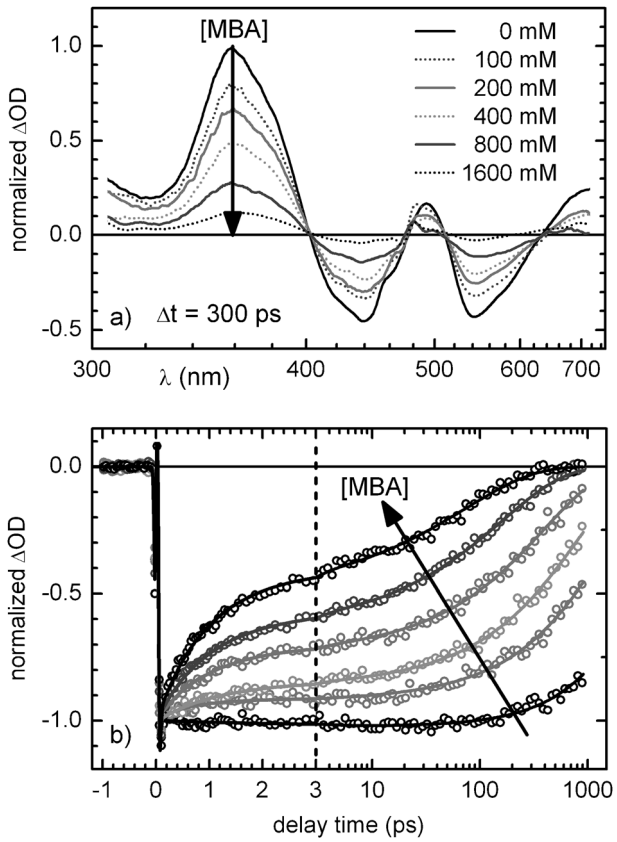

Fig. 3 (a) TA spectra of RFTA in MeCN/DMSO (98 : 2, v/v) for different MBA concentrations at 300 ps delay. The spectra have been normalized to the initial amplitude of the ESA band after photo-excitation. (b) Decay of the SE of RFTA in MeCN/H_2O (50 : 50, v/v) for the same MBA concentrations as in (a). The kinetic traces are obtained from band integrals (525–625 nm, circles). The fit functions according to the diffusion model described in the text are shown as solid lines. The delay time axis is linear between −1 and 3 ps and logarithmic between 3 and 1000 ps.

In contrast to the situation in pure MBA, the SE now decays on the same timescale as the other signatures. The reason for this is that the reaction of ^{1}RFTA* with MBA is now a two-stage process: first, the reactants have to approach from a large separation distance to close proximity by diffusion and then the ET and all subsequent steps occur in this close configuration. If the concentration of MBA is not extremely high (<1 M), the rate to form an encounter pair of ^{1}RFTA* and MBA is much smaller than the first-order rate coefficient $^1k_{ET} = (4\ \text{ps})^{-1}$ of the ET and also smaller than the back reaction rate $^1k_{b-ET} = (50\ \text{ps})^{-1}$ (see Section 3.1). Hence, the observed dynamics are governed by the diffusion limited formation of ^{1}RFTA*–MBA-encounter pairs that lead to a non-productive deactivation of ^{1}RFTA* by an ET cycle like in pure MBA. Again, this model is qualitatively confirmed by the absence of any product signals at long delays for the highest MBA concentrations.

For a quantitative modeling of the diffusion dynamics, the use of single or multi-exponential fit functions is generally not justified. In the case of diffusive quenching, the intensity decay becomes non-exponential due to a time dependence of the reaction rate.[49,50] The transient effect originates from a changing concentration of MBA quenchers around the excited RFTA molecules. The concentration is directly related to the average distance between the reactants and thereby to the time needed for an encounter after a random walk. Following excitation, the RFTA chromophores with nearby quenchers from the statistical distribution will react first. At later times, the ensemble of left over excited flavins faces a smaller effective MBA concentration and reacts with a smaller rate. At some point, the depletion of the MBA density around the remaining RFTA* molecules is balanced by the diffusion of bulk MBA molecules towards RFTA*. Thus, the reaction rate decreases from an initially high value to a constant that depends on the mutual diffusion coefficient D and the interaction distance R_{int} of the molecules.

The derivation of the mathematical description of this model follows ref. 49. It starts from Fick's law of diffusion for the MBA quencher molecules:

$$\frac{\partial \rho_{MBA}(r,t)}{\partial t} = D\nabla^2 \rho_{MBA}(r,t) \qquad (3)$$

The concentration of MBA quencher molecules is described by the normalized density distribution ρ_{MBA} around a spherical RFTA* molecule at $r = 0$. The diffusion equation contains three partial derivatives, the general solution therefore requires one initial condition at fixed time and two boundary conditions for fixed space coordinates. In the Smoluchowski theory, the initial condition is used that at the moment of excitation ρ_{MBA} is homogeneous around any RFTA molecule, *i.e.* $\rho_{MBA}(r, t = 0) = 1$ for $r > R_{int}$, but no reactant separation smaller than the interaction distance R_{int} is possible, *i.e.* $\rho_{MBA}(r, t = 0) = 0$ for $r \leq R_{int}$. One boundary condition is obtained by assuming that the bulk concentration of quenchers far away from the excited chromophore is not affected by the reaction, *i.e.* $\rho_{MBA}(r \to \infty, t) = 1$. The second boundary condition follows from the fact that no quencher molecules are found at a distance R_{int} from the excited chromophores at any time, *i.e.* $\rho_{MBA}(R_{int}, t) = 0$.

Solving eqn (3) under these conditions and substituting the result into the particle current of MBA molecules through a surface of area $4\pi R_{int}^2$ yields the reaction rate of MBA quenchers with the excited RFTA* molecules:[49]

$$-\frac{d[RFTA^*]}{dt} = 10^3 N_A 4\pi R_{int} D\left(1 + \frac{R_{int}}{\sqrt{\pi D t}}\right)[MBA]_0[RFTA^*] = k_{diff}(t)[MBA]_0[RFTA^*] \qquad (4)$$

$[MBA]_0$ and [RFTA*] are the initial concentrations of MBA and excited RFTA molecules in the solution. The multiplication with 10^3 N_A where N_A is Avogadro's number is needed to convert $k_{diff}(t)$ to units of $M^{-1}\ s^{-1}$.

The change in optical density $\Delta OD(t)$ observed in our transient experiments is proportional to [RFTA*](t). Integrating eqn (4) therefore yields an expression that can be used directly to model the diffusion controlled fluorescence quenching:

$$\Delta OD(t) = \Delta OD(0)\exp\left\{-\frac{t}{\tau_{fl}} - 10^3 N_A 4\pi R_{int} D[MBA]_0\left(1 + \frac{2R_{int}}{\sqrt{\pi D t}}\right)t\right\}. \qquad (5)$$

Table 1 Results of the fit to the femtosecond TA data for varying MBA concentrations in two solvent mixtures using the diffusion model. The exponential contribution from pre-associated aggregates yielded τ_{fast}(SE) = 4.5 ps and τ_{fast}(ESA) = 36 ps in MeCN/DMSO and τ_{fast}(SE) = 0.9 ps and τ_{fast}(ESA) = 6.4 ps in MeCN/H_2O. The resulting interaction radii were 3.8 Å and 6.0 Å, respectively.

[MBA]/mM	100	200	400	800	1600
	MeCN/DMSO (98 : 2)				
A_{fast}/A_{diff}	0.05	0.06	0.09	0.16	0.25
D/Å^2 ns^{-1}	160	130	110	100	90
$\tau_{fl,eff}$/ps	1100	740	420	230	87
$\Phi_{ISC}/\Phi_{ISC,0}$ (%)	18	12	7.0	3.8	1.5
	MeCN/H_2O (50 : 50)				
A_{fast}/A_{diff}	0.07	0.17	0.32	0.57	0.95
D/Å^2 ns^{-1}	59	60	56	52	42
$\tau_{fl,eff}$/ps	1400	700	310	120	45
$\Phi_{ISC}/\Phi_{ISC,0}$ (%)	23	12	5.2	2.0	0.75

Here, τ_{fl} is the fluorescence lifetime of RFTA, and $D = D_{RFTA} + D_{MBA}$ is the mutual diffusion constant.

The Smoluchowski diffusion model provides a consistent description of the predominant contribution to the dynamics for all MBA concentrations and over the whole spectral range. For the quantitative modeling, we preferred band integrals over transients at individual wavelengths. This minimizes the influence of spectral diffusion caused for instance by solvation or vibrational cooling. For a given MBA concentration, the diffusion dynamics in all three major bands (ESA, GSB and SE) could be described by one common set of parameters. The obtained values are given in Table 1.

In MeCN/DMSO solution, the mutual diffusion constant D of RFTA and MBA was found to lie between 90 and 160 Å^2 ns^{-1}. This is in good agreement with the values estimated from the Stokes–Einstein relationship for spherical particles with radius R in a solution of viscosity η at the absolute temperature T:

$$D = \frac{k_B T}{6\pi\eta}\left(\frac{1}{R_{RFTA}} + \frac{1}{R_{MBA}}\right) \geq \frac{k_B T}{6\pi\eta R_{MBA}}. \qquad (6)$$

From its bulk properties, R_{MBA} can be estimated to 3.7 Å, while η of pure MeCN at room temperature is 0.34 mPa s[51] yielding $D \geq 170$ Å^2 ns^{-1}. In the presence of DMSO and upon addition of MBA, the viscosity of the solution rises and D decreases accordingly (see Table 1).

As expected, the interaction distance R_{int} was not found to change for different MBA concentrations within the accuracy of our experiment. Interestingly, the obtained value of 3.8 Å is significantly smaller than the sum of the molecular radii of RFTA and MBA. This indicates that a specific orientation, most likely a face-to-face geometry, is required for an efficient electron transfer.[52,53]

For low MBA concentrations, the agreement between the diffusion model and our transient data is quite satisfactory. However, at higher MBA concentrations we observe an additional very fast component in the flavin kinetics. Since the Smoluchowski theory already poses an upper bound for the reaction rate at contact,[54] this cannot be due to the simplifying assumptions of the diffusion fit function. For a consistent modeling at all MBA concentrations, we therefore added an exponential term with a ps decay time to the fit function. As shown in Table 1, the relative amplitude A_{fast} of this component rises with the MBA concentration. It can therefore be assigned to preassociated RFTA–MBA aggregates[54,55] which are not subject to diffusion control.

This assignment is supported by the characteristic decay time τ_{fast} obtained from the fit: it is not dependent on the MBA concentration and it is smaller in the spectral region of the SE (4.5 ps) than in the ESA band (36 ps). This reflects the forward and backward electron transfer times in the aggregates, in agreement to the situation of RFTA dissolved in pure MBA. From the relative aggregate contribution at different MBA concentrations, one can calculate an association constant of $K = 0.2$ M^{-1} for RFTA–MBA-complexes in MeCN/DMSO solution. This value is even smaller than the weak association constants around 1 M^{-1} found for other aromatic molecules of similar size in MeCN solution.[56] We assume that the aggregates consist of a π-stacked configuration of RFTA and MBA whose driving force is the hydrophobicity of the chromophores.

A careful check of the steady state absorption spectrum at varying MBA concentration in the RFTA solution did not render significant changes relative to the variation induced by changes in the polarity of the solvent. This is not unexpected considering the weak association constant and the large energy difference between the lowest RFTA excitation and the lowest MBA excitation.

Overall, the Smoluchowski diffusion model extended by the contribution from preassociated aggregates completely describes the observed dynamics of RFTA and MBA in dilute solution. Thus, no indications for a significant catalytic photooxidation of MBA to the aldehyde can be found, at least not for the MBA concentrations that are compatible with ultrafast spectroscopy. The higher this concentration, the faster the quenching of the S_1 state of RFTA by ET from MBA, which is then followed by rapid charge recombination.

3.3 Changes to the femtosecond dynamics upon the addition of water

From earlier studies[17] it is known that the quantum yield of flavin-catalyzed photooxidation of benzylic alcohol can rise significantly in the presence of water. We therefore performed a series of additional measurements in MeCN/H_2O (50 : 50, v/v) solution. Overall, we find similar spectral signatures and dynamics as in MeCN/DMSO. Again, an increase of the MBA concentration leads to a faster quenching of the RFTA fluorescence and an essentially concerted decay of all other transient signatures. The same diffusion model with an additional contribution from preassociated RFTA–MBA aggregates could be used to reach a consistent quantitative description of the dynamics (see Fig. 3b). However, the set of parameters had to be altered in comparison to the MeCN/DMSO solution.

First, the contribution of preassociated RFTA–MBA aggregates is now considerably higher. At 1600 mM MBA, the ratio of RFTA molecules in aggregates to free ones approaches 1 : 1 (see Table 1). The obtained association constant of $K' = 0.6$ M^{-1} is three times higher than in the absence of water. This confirms the hydrophobic effect as a driving force for the aggregation: this effect is of course stronger in the protic and

more polar solvent mixture including water.[56] The characteristic times for the forward (0.9 ps, SE band) and backward ET (6.4 ps, ESA band) inside the aggregates are smaller than in the MeCN/DMSO solution. This might be due to an interaction with the water molecules, *e.g.*, *via* hydrogen bonds that induce a favorable orientation of MBA and RFTA in the aggregates.

Secondly, the parameters of the Smoluchowski diffusion model are also slightly different in the presence of water. We find smaller mutual diffusion constants that indicate a larger effective radius of the moving particles (see eqn (6)). This means that RFTA and MBA probably diffuse together with their solvent shell. A slowed down diffusion of MBA through the last solvent layer around RFTA might add to the effect.[55] The increased amount of "bound" solvent molecules is also supported by the larger interaction distance of 6 Å.[52]

Whereas the obtained parameters from the diffusion model give rich insight into the processes on the molecular level, they are difficult to be interpreted in terms of relevant timescales. To obtain a graspable measure for the reaction dynamics at the different MBA concentrations in both solvent mixtures, we determined an effective fluorescence lifetime $\tau_{fl,eff}$ from the normalized integral over the change in signal $\Delta OD(SE; t)$ in the range of the stimulated emission:[57]

$$\tau_{fl,eff} = \frac{1}{\Delta OD(SE;0)} \int_{t=0}^{\infty} \Delta OD(SE;t)dt. \qquad (7)$$

This measure is meaningful, as it recovers the decay time for a simple exponential decay as well as the weighted average for a multi-exponential and increases monotonically for longer complex decays. The results are given in Table 1. For technical reasons the values are most reliable for the high MBA concentrations. Their faster dynamics can be observed better within our fixed time window and therefore less extrapolation is required. Nevertheless, the comparison of MeCN/DMSO with MeCN/H_2O shows that the difference of the reaction speed decreases towards smaller MBA concentrations and eventually changes sign. At 1600 mM, the higher amount of aggregation in the presence of water outweighs the slower diffusion dynamics resulting in half the effective fluorescence lifetime. In contrast, at 100 mM MBA (and below), the contribution from RFTA–MBA-aggregates can be neglected and the speed of the diffusion is the only relevant parameter. Then, the smaller diffusion constants in the aqueous environment lead to a larger fluorescence lifetime than in MeCN/DMSO.

3.4 Dynamics involving the triplet state of RFTA

The findings presented above show no photooxidation of MBA as long as the forward and backward ET happen in the singlet manifold. As shown explicitly for RFTA in three different environments (pure MBA, MeCN/DMSO and MeCN/H_2O), the ET reaction of MBA with ^{1}RFTA* is followed by rapid charge recombination. The relevance of this loss channel is lowered when the MBA concentration is decreased. Indeed the chemical conversion was reported at 2 mM,[11] much lower than the concentrations used in the femtosecond measurements. With lower MBA concentration, the probability for intersystem crossing of the excited RFTA rises. A measure of the quantum yield of triplet formation Φ_{ISC} relative to the intrinsic yield $\Phi_{ISC,0}$ in the absence of MBA is given by the ratio between $\tau_{fl,eff}$ and the native fluorescence lifetime of RFTA of 6.0 ns. As shown in Table 1, Φ_{ISC} is higher in the presence of water for MBA concentrations below 100 mM which could contribute to the increased reaction quantum yield in buffer solution found at low substrate concentrations.[17]

To accentuate the spectral signature of ^{3}RFTA with our femtosecond setup, we redirected the pump light and omitted the prism compressor and the delay stage. The shortened optical path of the pump pulses resulted in a fixed delay of 12 ns for the white light probe, twice the fluorescence lifetime of flavin. As shown in Fig. 4, the transient spectrum of RFTA in pure MeCN/H_2O solution measured in this way (dotted line) differs significantly from the S_1 spectrum obtained shortly after excitation (Δt = 300 fs, dashed line). On the short wavelength side, the absorption maximum shifts by 2200 cm^{-1} from 358 nm to 388 nm. A comparison with the GSB band shows that the extinction coefficient of the ESA band has dropped by roughly a factor of three.

On the long wavelength side above 500 nm, the negative signature from the stimulated emission is largely missing in the 12 ns transient. Instead, a broad absorption is observed with a double peak around 650 and 710 nm and a smaller peak at 510 nm. This is in good agreement with published triplet spectra of similar flavin compounds.[43,58] When MBA is added to the solution (solid line), the amplitude of all signatures decreases, in analogy to the situation at 300 ps delay shown in Fig. 3a. A normalization to the GSB minimum shows that even at 12 ns delay the transient of RFTA without MBA has the expected weak contribution from ^{1}RFTA* as seen from the higher absorption around 360 nm and the lower one in the SE region (see Fig. 4) compared to the spectrum with 50 mM MBA.

The dynamics of the triplet state proceed on a nano- to microsecond timescale. This range cannot be covered with the femtosecond setup and transient data were therefore measured with the Streak-camera setup. The obtained spectra at short delay times <1 μs are identical with the 12 ns spectra

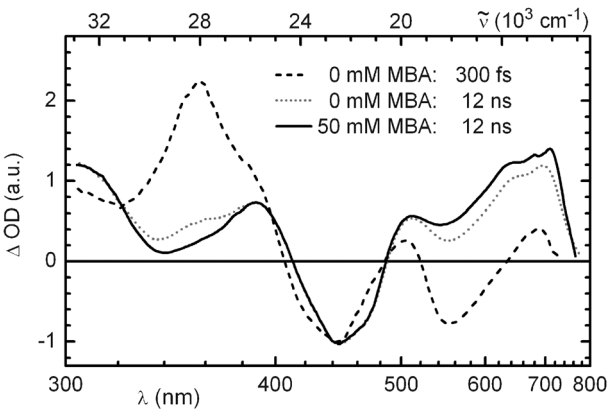

Fig. 4 Transient absorption spectra of RFTA in MeCN/H_2O (50 : 50, v/v) directly after excitation (singlet state; dashed line) and after 12 ns delay (triplet state; dotted and solid lines). The spectra have been normalized to the ground state absorption minimum.

from the fs-setup. However, in striking contrast to the unproductive singlet reaction observed in the ultrafast experiments, the μs measurements reveal a productive reaction between MBA and ^{3}RFTA beyond the forward and back-ET. This is most clearly seen as a persistent signature on the 10 μs scale that agrees well with the neutral protonated flavin radical RFTAH$^\bullet$ (for details see below).

Without MBA in the solution, the TA signal from ^{3}RFTA decays monoexponentially with τ = 1.3 μs (data not shown). The corresponding rate of 7.7×10^5 s^{-1} reflects the diffusional triplet quenching by oxygen in the solution and compares well to similar systems reported in the literature.[24,59,60] Upon addition of MBA, the observed dynamics show significant changes.

Fig. 5 shows the data obtained with 40.9 μM RFTA and 50 mM MBA in MeCN/$H_2$0 (50 : 50, v/v) solution after excitation at 445 nm. Panel a shows a false colour map of the 2D-transient absorption data matrix. Panel b shows times traces at various wavelengths: the line in magenta represents the time profile of the pump pulse corresponding to the instrument response function. The red dots (700 nm) can be assigned to absorption of the triplet state, decaying with a lifetime of 700 ns. Bleaching at 450 nm (black dots) only recovers partially on this scale. The rise and decay of the green dots (520) and the blue dots (350 nm) indicate the presence of transient intermediates.

A model which contains, in addition to the instrument response function, two exponential functions and one constant term was found suitable to fit the data (Table 2). The fit yields the fluorescence spectrum (associated with the instrument response, not shown) and three decay associated difference spectra (DADS) shown in panels c–e. From the fastest time constant and the intrinsic triplet lifetime in the presence of oxygen we calculated a quenching constant of $^3k_{ET} = 1.3 \times 10^7$ M^{-1} s^{-1} corresponding to an ET from MBA to ^{3}RFTA. The corresponding DADS reflects the conversion of ^{3}RFTA to RFTA$^{\bullet-}$ (see Fig. 5c) as seen from the disappearance of the broad long-wavelength absorption and a blueshift of the maximum at ~370 nm.[43] The radical ion pair RFTA$^{\bullet-}$ and MBA$^{\bullet+}$ has two deactivation pathways: back-ET to the ground state of the system and the productive proton transfer from MBA to flavin yielding a neutral radical pair. The sum of these two rates was fitted to 1.8×10^5 s^{-1}, corresponding to a lifetime of the ion pair of 5.5 μs in accordance with previous studies.[46,61] According to our model, flavin and MBA are in contact—or at least close proximity—after the initial ET. Therefore, the decay of the ion pair should not depend on the substrate concentration. We find a small increase of the effective ion pair lifetime by a factor of 2 when the MBA concentration is increased by a factor of 10 from 50 mM to 500 mM.

In our detection window of up to 20 μs, we observe the signature of a non-decaying species displaying a broad absorption between 500 and 600 nm and a maximum around 350 nm (see Fig. 5e). The signature can be assigned to the neutral protonated flavin radical RFTA–H$^\bullet$.[43,58,62] This confirms the proposed mechanism of ET followed by a proton transfer between MBA and flavin in the triplet state.

We thus propose that the measurement in the 10 μs range reflects the following reaction steps: The initially populated

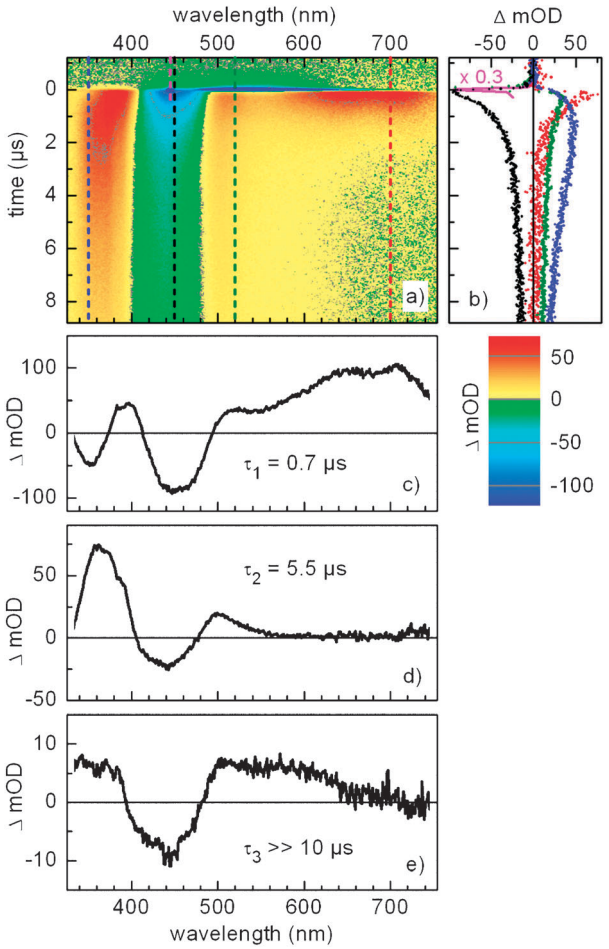

Fig. 5 (a) False colour map of the 2D-transient absorption data matrix measured with 40.9 μM RFTA and 50 mM MBA in MeCN/H_2O (50 : 50, v/v) solution after excitation at 445 nm. (b) Time traces at various wavelengths. (c–e) Decay associated difference spectra from the global fit.

Table 2 Results of the global fit to the streak camera measurements for varying MBA concentrations. $\tau_1 = (k_{b-ISC} + {}^3k_{ET}[MBA])^{-1}$; $\tau_2 = (k_{PT} + {}^3k_{b-ET})^{-1}$; $\tau_3 = (k_{prod})^{-1}$. For [MBA] = 0 mM: $\tau_1 = (k_{b-ISC})^{-1} = (7.7 \times 10^5\ s^{-1})^{-1}$

[MBA]/mM	τ_1/μs	$^3k_{ET}$/M^{-1} s^{-1}	τ_2/μs	τ_3/μs
0	1.3	—	—	—
2	1.2	3.2×10^7	—	—
20	0.92	1.6×10^7	4.1	≫10
50	0.70	1.3×10^7	5.5	≫10
100	0.57	0.99×10^7	6.3	≫10
200	0.31	1.2×10^7	8.0	≫10
500	0.09	2.1×10^7	11	≫10

triplet state decays with a total rate constant k_1. A fraction α of this decays into the radical anion RFTA$^{\bullet-}$, whereas a fraction $(1 - \alpha)$ decays back to the ground state. Similarly, the total decay of RFTA$^{\bullet-}$ occurs with rate constant k_2 with a fraction β forming the neutral radical RFTA–H$^\bullet$ and a fraction $(1 - \beta)$ falling back to the ground state. The decay associated difference spectra DADS$_1$, DADS$_2$, and DADS$_3$ (see Fig. 5) corresponding to the three rate constants k_1, k_2, and $k_3 \approx 0$ are then

expressed in terms of the species associated difference spectra $SADS_{triplet}$, $SADS_{neutral\ radical}$ and $SADS_{radical\ anion}$ by:

$$DADS_1 = SADS_{triplet} + \frac{\alpha}{k_1 - k_2}(k_2\beta \cdot SADS_{neutral\ radical} - k_1 \cdot SADS_{radical\ anion})$$

$$DADS_2 = \frac{\alpha k_1}{k_1 - k_2}(SADS_{radical\ anion} - \beta \cdot SADS_{neutral\ radical})$$

$$DADS_3 = \alpha\beta \cdot SADS_{neutral\ radical} \quad (8)$$

This system of linear equations can be inverted to yield the SADS but the inversion requires knowledge of the fractions α and β, which cannot be determined by a fit to the data:

$$SADS_{triplet} = DADS_1 + DADS_2 + DADS_3$$

$$SADS_{radical\ anion} = (DADS_3 + DADS_2\,(1 - k_2/k_1))/\alpha \quad (9)$$

$$SADS_{neutral\ anion} = DADS_3/(\alpha\beta)$$

The fraction α, however, can be calculated from the total decay rate constants of the triplet in the absence (k_0) and in the presence (k_1) of MBA as $\alpha = 1 - k_0/k_1$. For an MBA concentration of 50 mM we find $\alpha = 0.46$. The fraction β only enters in the expression for $S_{neutral\ radical}$ as a scaling parameter. The true species associated spectra (SAS) can be obtained from the SADS by adding the ground state spectrum in an appropriate amount depending on the excitation conditions. Fig. 6 shows the SAS of the three intermediate flavin states obtained from the data at 50 mM MBA and assuming $\beta = 0.3$. The SAS are in very good agreement with previously reported absorption spectra of flavin in the triplet state, the semiquinone radical anion and the protonated neutral radical state.[43]

The proposed sequential electron and proton transfer is also confirmed by experiments at different pH values. Under acidic conditions (addition of 1 mM HCl to the sample solution), we observed no radical anion anymore, but immediately ($\Delta t \approx 50$ ns) the formation of the neutral radical out of the triplet state. In contrast, under alkaline conditions (addition of 1 mM NaOH to the sample solution) no neutral radical could be seen, but only the radical anion form of RFTA.

In our experiments we cannot yet observe the final step of the reaction yielding the fully reduced flavin and the MB-aldehyde. The required hydrogen atom transfer or disproportionation reactions likely occur on slower timescales up to the ms regime.[63]

3.5 Mechanism of the photocatalytic MBA oxidation

From the spectroscopic studies on the various timescales we can compile a detailed scheme of the photooxidation mechanism of MBA in the presence of RFTA (Fig. 7). The rapid, non-productive forward and back-ET from the singlet state of flavin is opposed by the productive stepwise redox reaction involving the triplet state of flavin. The complete picture is confirmed by the non-trivial dependence of the reaction quantum yield (QY) on the substrate concentration shown in Fig. 8. The relative QY for the various concentrations was measured by illumination with a high power LED, the absolute

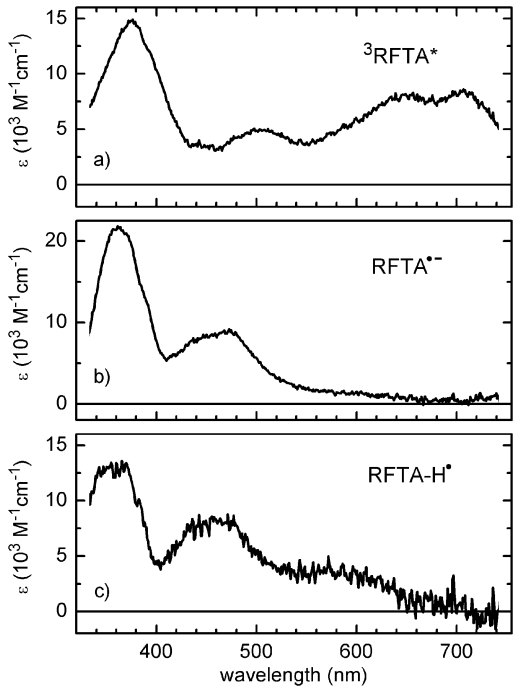

Fig. 6 Species Associated Spectra (SAS) resulting from the proposed model using the Decay Associated Difference Spectra (DADS) from the global fit analysis. The used parameters were: $\alpha = 0.46$, $\beta = 0.3$ and $SAS_{ground\ state} = 0.3\ S_0$ as the fraction of ground state which was added.

QY by subsequent gas chromatographic detection of the chemical conversion.[20] For a productive singlet channel, one would expect that the QY increases monotonically with the MBA concentration and reaches a constant value at some point.[6–8] However, we find a completely different behavior with a maximum QY of 3% at 25 mM MBA. For both lower and higher MBA concentrations we observe a significant drop of the QY. This can be well understood with our model. At high MBA concentrations, the required ISC to ^{3}RFTA cannot occur due to fast and non-productive S_1 quenching by MBA. At concentrations below 25 mM, the diffusional approach of MBA and RFTA is becoming slow compared to the intrinsic triplet lifetime. Thus, a balance of the diffusion timescale—*via* the MBA concentration—and the ISC rate is necessary in order to have an encounter of the reactants at the right time: when RFTA is not in the singlet state any more but has not yet relaxed from the triplet state either.

To model quantitatively the dependence of the reaction quantum yield Φ_{tot} on the MBA concentration we use the fit results from the spectroscopic experiments to deduce the QYs of the individual productive steps, *i.e.* intersystem crossing, electron transfer and proton transfer:

$$\Phi_{tot} \le \Phi_{ISC}\Phi_{ET}\Phi_{PT} \le \frac{k_{ISC}}{\tau_{fl}^{-1} + {}^1k_{ET}[MBA]} \frac{{}^3k_{ET}[MBA]}{{}^3k_{ET}[MBA] + k_{b-ISC}} \frac{k_{PT}}{{}^3k_{b-ET} + k_{PT}} \quad (10)$$

The less than or equal sign in eqn (10) refers to the fact that the last step of the reaction, which at the moment lies beyond our

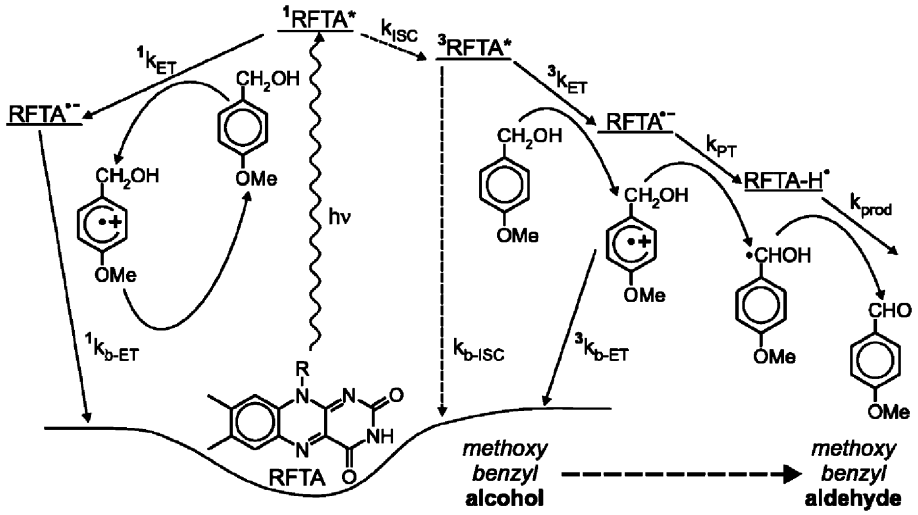

Fig. 7 Scheme of the oxidation mechanism of MBA. The non-productive singlet channel (left hand side) brings the excited RFTA back to the ground state after diffusion controlled electron transfer from MBA ($^1k_{ET}$) and fast charge recombination ($^1k_{b-ET}$). The encounter of MBA with a triplet flavin (right hand side) can eventually lead to product formation *via* a sequence of electron and proton transfer events. Details see text.

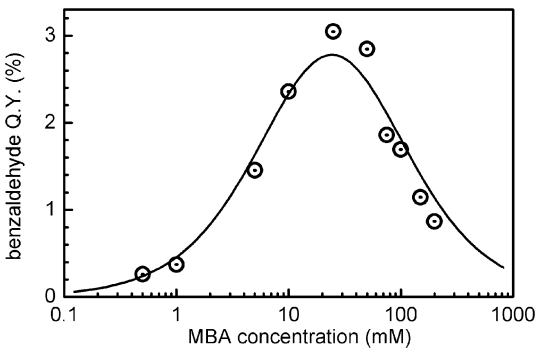

Fig. 8 Circles: Quantum yield of benzaldehyde production in MeCN/H_2O (50 : 50, v/v) solution. Solid line: Simulation using the spectroscopically determined reaction rates.

spectroscopically accessible timescale, could further reduce the total QY. The QYs of intersystem crossing Φ_{ISC} and electron transfer in the triplet state Φ_{ET} depend on the following known rates:

$(\tau_{fl})^{-1} = (6.0\ ns)^{-1} = 1.7 \times 10^8\ s^{-1}$ (from a TCSPC measurement of the ^{1}RFTA* fluorescence)

$^1k_{ET} = 1.3 \times 10^{10}\ M^{-1}\ s^{-1}$ (from a linear fit to $\tau_{fl,eff}$ at different MBA concentrations)

$^3k_{ET} = 1.7 \times 10^7\ M^{-1}\ s^{-1}$ (from the μs decay dynamics at different MBA concentrations)

$k_{b-ISC} = 7.7 \times 10^5\ s^{-1}$ (from the decay of ^{3}RFTA* in the absence of MBA)

The QY of proton transfer Φ_{PT} corresponds to the parameter $\beta = 0.3$ that was used to obtain the SAS (see Section 3.4). Thus, k_{ISC} is the only free parameter that is not *a priori* known from the spectroscopic analysis. Since it only affects the amplitude of the QY function, the course of Φ_{tot} *vs.* MBA is fixed by the known parameters listed above. As shown in Fig. 8, the derived model (solid line) agrees very well with the measured QYs (circles). This confirms qualitatively and quantitatively the triplet reaction mechanism shown in Fig. 7.

From a least-square fit to the experimental QY data we obtain $k_{ISC} \geq 1.3 \times 10^8\ s^{-1}$. This corresponds to an intrinsic triplet yield of RFTA of 76% in the absence of MBA, which is among the highest values reported for other flavin compounds.[22,37,39] This implies that almost no losses occur in the photooxidation reaction after the first proton transfer step.

For the MeCN/DMSO solvent, *i.e.* in the absence of water, we reported a nearly hundred times lower reaction quantum yield.[20] In the light of the present discussion, we could interpret this as a dramatically reduced probability for proton transfer. It does not seem unlikely that the RFTA radical anion and the MBA radical cation separate by a few solvent molecules between their generation and the proton transfer. In the aqueous environment the hydrogen bond network could still give a good transfer yield, whereas the absence of proton mediators would make this step much more inefficient. One could even speculate that an increased MBA concentration leads to rather far reaching disturbance of the hydrogen network[64] and thereby explains the observed decrease of the proton transfer rate with the rising MBA concentration.

4. Conclusion and outlook

In this work we investigated the flavin-catalyzed photooxidation mechanism of MBA with transient absorption spectroscopy on a timescale ranging from sub-picoseconds to tens of microseconds. The results show that the productive reaction proceeds *via* the triplet state of RFTA and starts with a sequence of an electron and a proton transfer step from MBA to RFTA within 0.1 to 10 μs. In contrast, electron transfer to the singlet excited state of RFTA leads to rapid charge recombination within 50 ps and therefore constitutes a loss channel. Its relevance increases with substrate concentration since diffusion then allows for an encounter of MBA and the excited RFTA before ISC has occurred. In addition, we find a considerable contribution from preassociated RFTA–MBA-aggregates for high MBA concentrations of several 100 mM that also undergo a fast and unproductive

charge separation and recombination cycle. Thus, at high substrate concentrations and especially in pure MBA solution, no significant product formation is observed.

However, if the first ET proceeds after the ISC of RFTA, the charge recombination in the spin correlated radical ion pair is spin forbidden and therefore significantly slowed down.[65] This allows for a higher efficiency of the second reaction step, *i.e.* the proton transfer from $MBA^{\bullet+}$ to $RFTA^{\bullet-}$. For a high product QY, the average distance between MBA and RFTA has to be large enough to prevent the likely diffusional encounter within the singlet state lifetime of RFTA which can be achieved by using lower substrate concentrations.

The detailed mechanistic study reveals that the design of a photocatalyst based on the assumption of close proximity of the redox active chromophore and the substrate binding site is not valid for flavins. Instead, other approaches are conceivable to obtain new photocatalysts with improved performance. One possibility is to try to increase the triplet yield by acceleration of the ISC. This might be achieved by exploiting the heavy atom effect through suitable substitution on the flavin chromophore, for instance with sulfur containing groups.[66] Additional substitution of flavin with bulky side chains might impede the aggregation with the substrate by steric hindrance. This would also lead to a higher fraction of excited flavin molecules that can access the triplet state. Another possibility is to use triplet sensitizers[67] that undergo rapid ISC and then transfer their triplet energy to flavin. Thus, the singlet loss channel could be completely circumvented, however with the likely drawback of a higher excitation energy, *i.e.* with the need for UV illumination instead of the desired visible light for the photocatalysis. Performance of the reaction under anaerobic conditions seems tempting, since it would prolong the triplet lifetime. However, oxygen is needed for the reoxidation of RFTA to restore the catalyst. A nearly anaerobic situation might increase the QY at low MBA concentrations, but it would only allow for a very slow overall chemical conversion.

A more promising approach might be to work at high substrate concentrations and render the singlet channel productive. This implies the inhibition of the unproductive back-ET and/or the acceleration of the further productive reaction steps. A concept for this can be found in the general architecture of natural proteins that are involved in redox reactions.[68] There, one frequently finds multiple redox centers in close proximity to each other. By efficient separation of the induced charges along a chain of reaction centers, the charge recombination as well as other deactivation pathways is outpaced. For the flavin photocatalysis, this could imply the attachment of an intermediate electron acceptor unit to the chromophore that also acts as a substrate binding site. After the initial electron transfer from MBA to the intermediate redox center, the negative charge could then be transferred to the flavin. This might slow down the unproductive back electron transfer in favor of subsequent proton and electron transfer events from MBA to the catalyst. Indeed, ten times higher product quantum yields up to 40% were found for the photooxidation of benzylic alcohol using a flavin compound with a covalently linked zinc(II)-cyclen binding site.[17] Further investigations on the details of the reaction mechanism with this catalyst are needed, as well as an improvement of its photostability. However, the insights from the reaction mechanism of RFTA with MBA described in this work encourage further research along this line to reach higher efficiencies for photocatalytic chemical conversions.

Acknowledgements

We thank the Deutsche Forschungsgemeinschaft (GRK 1626, SFB 749 and GRK 640) for support of our research. We gratefully acknowledge financial support from the International Max Planck Research School on Advanced Photon Science (U.M.). Discussions with B. Fingerhut and C. F. Sailer were stimulating.

References

1 *Flavins: Photochemistry and Photobiology*, ed. E. Silva and A. M. Edwards, Royal Society of Chemistry, Cambridge, 2006.
2 W. Tong, H. P. Ye, H. H. Zhu and V. T. D'Souza, *THEOCHEM*, 1995, **333**, 19–27.
3 Y. Yano, *Rev. Heteroat. Chem.*, 2000, **22**, 151–179.
4 S. Shinkai, K. Kameoka, K. Ueda, O. Manabe and M. Onishi, *Bioorg. Chem.*, 1987, **15**, 269–282.
5 S. Shinkai, K. Kemeoka, K. Ueda and O. Manabe, *J. Am. Chem. Soc.*, 1987, **109**, 923–924.
6 S. Fukuzumi, S. Kuroda and T. Tanaka, *J. Am. Chem. Soc.*, 1985, **107**, 3020–3027.
7 S. Fukuzumi and S. Kuroda, *Res. Chem. Intermed.*, 1999, **25**, 789–811.
8 S. Fukuzumi, K. Yasui, T. Suenobu, K. Ohkubo, M. Fujitsuka and O. Ito, *J. Phys. Chem. A*, 2001, **105**, 10501–10510.
9 E. Silva, A. M. Edwards and D. Pacheco, *J. Nutr. Biochem.*, 1999, **10**, 181–185.
10 A. Mees, C. Behrens, A. Schwögler, M. Ober and T. Carell, *Eur. J. Org. Chem.*, 2003, 2670–2677.
11 J. Svoboda, H. Schmaderer and B. König, *Chem.–Eur. J.*, 2008, **14**, 1854–1865.
12 H. Schmaderer, P. Hilgers, R. Lechner and B. König, *Adv. Synth. Catal.*, 2009, **351**, 163–174.
13 S. Shinkai, G. X. He, T. Matsuda, A. D. Hamilton and H. S. Rosenzweig, *Tetrahedron Lett.*, 1989, **30**, 5895–5898.
14 B. König, M. Pelka, R. Reichenbach-Klinke, J. Schelter and J. Daub, *Eur. J. Org. Chem.*, 2001, 2297–2303.
15 M. Gray, A. J. Goodman, J. B. Carroll, K. Bardon, M. Markey, G. Cooke and V. M. Rotello, *Org. Lett.*, 2004, **6**, 385–388.
16 A. S. F. Boyd, J. B. Carroll, G. Cooke, J. F. Garety, B. J. Jordan, S. Mabruk, G. Rosair and V. M. Rotello, *Chem. Commun.*, 2005, 2468–2470.
17 R. Cibulka, R. Vasold and B. König, *Chem.–Eur. J.*, 2004, **10**, 6223–6231.
18 R. Lechner and B. König, *Synthesis*, 2010, 1712–1718.
19 J. Svoboda and B. König, *Chem. Rev.*, 2006, **106**, 5413–5430.
20 U. Megerle, R. Lechner, B. König and E. Riedle, *Photochem. Photobiol. Sci.*, 2010, **9**, 1400–1406.
21 R. Kuhn, P. Gyorgy and T. Wagner-Jauregg, *Ber. Dtsch. Chem. Ges. B*, 1933, **66**, 576–580.
22 P. F. Heelis, *Chem. Soc. Rev.*, 1982, **11**, 15–39.
23 R. J. Stanley and A. W. MacFarlane, *J. Phys. Chem. A*, 2000, **104**, 6899–6906.
24 C. Y. Lu, G. Bucher and W. Sander, *ChemPhysChem*, 2004, **5**, 47–56.
25 Y. T. Kao, C. Saxena, T. F. He, L. J. Guo, L. J. Wang, A. Sancar and D. P. Zhong, *J. Am. Chem. Soc.*, 2008, **130**, 13132–13139.
26 A. Weigel, A. L. Dobryakov, M. Veiga and J. L. P. Lustres, *J. Phys. Chem. A*, 2008, **112**, 12054–12065.
27 C. Aubert, M. H. Vos, P. Mathis, A. P. M. Eker and K. Brettel, *Nature*, 2000, **405**, 586–590.
28 D. P. Zhong and A. H. Zewail, *Proc. Natl. Acad. Sci. U. S. A.*, 2001, **98**, 11867–11872.

29 T. Kottke, J. Heberle, D. Hehn, B. Dick and P. Hegemann, *Biophys. J.*, 2003, **84**, 1192–1201.
30 M. Gauden, I. H. M. van Stokkum, J. M. Key, D. C. Lührs, R. Van Grondelle, P. Hegemann and J. T. M. Kennis, *Proc. Natl. Acad. Sci. U. S. A.*, 2006, **103**, 10895–10900.
31 A. Lukacs, A. P. M. Eker, M. Byrdin, K. Brettel and M. H. Vos, *J. Am. Chem. Soc.*, 2008, **130**, 14394–14395.
32 T. Langenbacher, D. Immeln, B. Dick and T. Kottke, *J. Am. Chem. Soc.*, 2009, **131**, 14274–14280.
33 K. Lanzl, M. von Sanden-Flohe, R. J. Kutta and B. Dick, *Phys. Chem. Chem. Phys.*, 2010, **12**, 6594–6604.
34 C. B. Martin, M. L. Tsao, C. M. Hadad and M. S. Platz, *J. Am. Chem. Soc.*, 2002, **124**, 7226–7234.
35 C. Neiss, P. Saalfrank, M. Parac and S. Grimme, *J. Phys. Chem. A*, 2003, **107**, 140–147.
36 E. Sikorska, I. Khmelinskii, A. Komasa, J. Koput, L. F. V. Ferreira, J. R. Herance, J. L. Bourdelande, S. L. Williams, D. R. Worrall, M. Insińska-Rak and M. Sikorski, *Chem. Phys.*, 2005, **314**, 239–247.
37 M. Insińska-Rak, E. Sikorska, J. L. Bourdelande, I. V. Khmelinskii, W. Prukała, K. Dobek, J. Karolczak, I. F. Machado, L. F. V. Ferreira, A. Komasa, D. R. Worrall and M. Sikorski, *J. Mol. Struct.*, 2006, **783**, 184–190.
38 K. Sadeghian, M. Bocola and M. Schütz, *J. Am. Chem. Soc.*, 2008, **130**, 12501–12513.
39 S. Salzmann, J. Tatchen and C. M. Marian, *J. Photochem. Photobiol., A*, 2008, **198**, 221–231.
40 S. Salzmann and C. M. Marian, *Photochem. Photobiol. Sci.*, 2009, **8**, 1655–1666.
41 G. Angulo, G. Grampp and A. Rosspeintner, *Spectrochim. Acta, Part A*, 2006, **65**, 727–731.
42 U. Megerle, I. Pugliesi, C. Schriever, C. F. Sailer and E. Riedle, *Appl. Phys. B: Lasers Opt.*, 2009, **96**, 215–231.
43 M. Sakai and H. Takahashi, *J. Mol. Struct.*, 1996, **379**, 9–18.
44 E. Baciocchi, M. Bietti, L. Putignani and S. Steenken, *J. Am. Chem. Soc.*, 1996, **118**, 5952–5960.
45 M. Bietti, E. Baciocchi and S. Steenken, *J. Phys. Chem. A*, 1998, **102**, 7337–7342.
46 E. Baciocchi, M. Bietti and S. Steenken, *Chem.–Eur. J.*, 1999, **5**, 1785–1793.
47 S. D. M. Islam, A. Penzkofer and P. Hegemann, *Chem. Phys.*, 2003, **291**, 97–114.
48 C. Reichardt, *Solvents and Solvent Effects in Organic Chemistry*, Wiley-VCH, Weinheim, 3rd edn, 2004.
49 S. A. Rice, *Diffusion-limited reactions*, Elsevier Science Publishers B.V., Amsterdam, 1985.
50 J. R. Lakowicz, *Principles of fluorescence spectroscopy*, Springer Science + Business Media, New York, 3rd edn, 2006.
51 J. H. Dymond, M. A. Awan, N. F. Glen and J. D. Isdale, *Int. J. Thermophys.*, 1991, **12**, 443–477.
52 S. G. Ballard and D. C. Mauzerall, *J. Chem. Phys.*, 1980, **72**, 933–947.
53 X. Allonas, P. Jacques, A. Accary, M. Kessler and F. Heisel, *J. Fluoresc.*, 2000, **10**, 237–245.
54 P. Sreearunothai, S. Asaoka, A. R. Cook and J. R. Miller, *J. Phys. Chem. A*, 2009, **113**, 2786–2795.
55 S. Pant, H. Ohtaka-Saiki, M. Takezaki, A. D. Scully, S. Hirayama and T. Tominaga, *J. Phys. Chem. A*, 2008, **112**, 5378–5384.
56 M. S. Cubberley and B. L. Iverson, *J. Am. Chem. Soc.*, 2001, **123**, 7560–7563.
57 M. N. Berberan-Santos, E. N. Bodunov and B. Valeur, *Chem. Phys.*, 2005, **315**, 171–182.
58 T. B. Melø, M. A. Ionescu, G. W. Haggquist and K. R. Naqvi, *Spectrochim. Acta, Part A*, 1999, **55**, 2299–2307.
59 C. B. Martin, X. F. Shi, M. L. Tsao, D. Karweik, J. Brooke, C. M. Hadad and M. S. Platz, *J. Phys. Chem. B*, 2002, **106**, 10263–10271.
60 B. Branchi, M. Bietti, G. Ercolani, M. A. Izquierdo, M. A. Miranda and L. Stella, *J. Org. Chem.*, 2004, **69**, 8874–8885.
61 E. Baciocchi, M. Bietti and S. Steenken, *J. Am. Chem. Soc.*, 1997, **119**, 4078–4079.
62 F. Müller, M. Brüstlein, P. Hemmerich, V. Massey and W. H. Walker, *Eur. J. Biochem.*, 1972, **25**, 573–580.
63 P. F. Heelis, B. J. Parsons, G. O. Phillips and J. F. McKellar, *Photochem. Photobiol.*, 1981, **33**, 7–13.
64 M. Heyden, E. Bründermann, U. Heugen, G. Niehues, D. M. Leitner and M. Havenith, *J. Am. Chem. Soc.*, 2008, **130**, 5773–5779.
65 J. W. Verhoeven, *J. Photochem. Photobiol., C*, 2006, **7**, 40–60.
66 P. Drössler, W. Holzer, A. Penzkofer and P. Hegemann, *Chem. Phys.*, 2003, **286**, 409–420.
67 L. Hviid, W. G. Bouwman, M. N. Paddon-Row, H. J. van Ramesdonk, J. W. Verhoeven and A. M. Brouwer, *Photochem. Photobiol. Sci.*, 2003, **2**, 995–1001.
68 C. C. Page, C. C. Moser, X. X. Chen and P. L. Dutton, *Nature*, 1999, **402**, 47–52.

